
An End-to-End Approach for Training Neural Network Binary Classifiers on Metrics Based on the Confusion Matrix

Nathan Tsoi, Kate Candon, Yofti Milkessa, Marynel Vázquez
Yale University, New Haven, CT 06511
nathan.tsoi@yale.edu

Abstract

While neural network binary classifiers are often evaluated on metrics such as Accuracy and F_1 -Score, they are commonly trained with a cross-entropy objective. How can this training-testing gap be addressed? While specific techniques have been adopted to optimize certain confusion matrix based metrics, it is challenging or impossible in some cases to generalize the techniques to other metrics. Adversarial learning approaches have also been proposed to optimize networks via confusion matrix based metrics, but they tend to be much slower than common training methods. In this work, we propose to approximate the Heaviside step function, typically used to compute confusion matrix based metrics, to render these metrics amenable to gradient descent. Our extensive experiments show the effectiveness of our end-to-end approach for binary classification in several domains.

1 Introduction

Neural network binary classifiers are often trained using a cross-entropy objective function. The network’s output is a probability $p \in [0, 1]$ that must be translated to a binary value $\{0, 1\}$ indicating set membership to the negative or positive class. To determine set membership, the Heaviside step function H is commonly used with a threshold τ , where $p \geq \tau$ are considered positive classification outcomes. This notion of set membership is often used in evaluation metrics for binary classifiers.

It is a common assumption that optimizing a network via the desired evaluation metric is preferable to optimizing a surrogate objective [10, 15, 33, 35]. However, the Heaviside function, commonly used to compute confusion matrix set membership in terms of true positives, false positives, false negatives, and true negatives, has a gradient with properties not conducive to optimization via gradient descent. The Heaviside function’s gradient is not defined at the threshold τ and is zero everywhere else (Fig. 1, left). Therefore the Heaviside function cannot be used to effectively backpropagate errors and train a neural network according to metrics composed of confusion matrix set values, such as F_1 -Score.

To address the aforementioned challenge, we propose a method to unify the training and inference steps for neural network binary classifiers. Specifically, we propose the use of a Heaviside step function approximation along with soft set membership to train these classifiers with confusion matrix based metrics as a loss function. We implement our method with an existing approximation (Fig. 1, middle). Also, we propose a novel linear approximation for H (Fig. 1, right), which approaches H in the limits for all threshold values, unlike the existing sigmoid approximation. Our method to train binary neural network classifiers is adaptable in that it can be combined with other common machine learning techniques, such as weighted sampling to help with class imbalance.

Our proposed approach is also unique in its flexibility to directly optimize any metric based on the confusion matrix with minimal changes to the objective function. This flexibility is important because the adequacy of a metric depends on the context of the problem, as well as the level of class imbalance of a dataset. For example, while Accuracy is a popular metric, it will over-estimate performance in

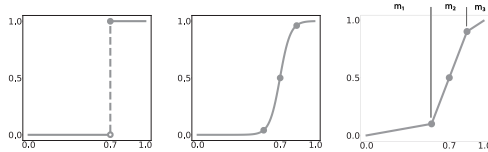


Figure 1: Heaviside function H (left), Sigmoid approximation \mathcal{H}^s [24] reparameterized with τ (middle), our novel Linear Heaviside function approximation \mathcal{H}^l (right), all at threshold $\tau = 0.7$.

datasets with high levels of class imbalance [14]. In these cases, the harmonic mean of precision and recall (F_1 -Score) is a better estimator. Our method can be easily adapted to both metrics.

Metrics based on confusion matrix set values are considered non-decomposable. Non-decomposable metrics cannot be calculated per datapoint and are not additive across subsets of data [19]. We acknowledge that our optimization method of mini-batch stochastic gradient descent (SGD) does not provide an unbiased estimator on non-decomposable metrics. However, this is common in neural network training [13]. In practice, we find that large enough mini-batches provide a representative sample for confusion matrix based metrics, allowing the use of mini-batch SGD in our approach. Moreover, our method does not limit maximum batch size for training, unlike the adversarial approach to optimize F_1 -Score proposed by [11].

In summary, our main contributions are: 1) a novel method for directly optimizing confusion matrix based metrics, 2) evaluation of two approximations of the Heaviside step function to facilitate batch gradient descent when training binary classifiers via our method, 3) empirical analysis of the practical effects of batch size when optimizing for metrics based on the confusion matrix sets, and 4) application of our approach to various domains, showing its flexibility and superior performance compared to several baseline methods. We provide implementations of our method in two deep learning frameworks for reproducibility.¹

2 Preliminaries

In binary classification via neural networks, a step function is required to transform the network’s output to a binary value. A common choice is the Heaviside step function with threshold value τ :

$$H(p, \tau) = \begin{cases} 1 & p \geq \tau \\ 0 & p < \tau \end{cases} \quad (1)$$

Confusion matrix set membership is then computed for a prediction p and ground truth label y via:

$$tp = \begin{cases} H(p, \tau) & y = 1 \\ 0 & \text{else} \end{cases} \quad fn = \begin{cases} 1 - H(p, \tau) & y = 1 \\ 0 & \text{else} \end{cases} \quad fp = \begin{cases} H(p, \tau) & y = 0 \\ 0 & \text{else} \end{cases} \quad tn = \begin{cases} 1 - H(p, \tau) & y = 0 \\ 0 & \text{else} \end{cases}$$

Consider a set of predictions $p \in [0, 1]$, ground truth labels $y \in \{0, 1\}$ and threshold value $\tau \in (0, 1)$, e.g., $\{(p_1, y_1, \tau), (p_2, y_2, \tau), \dots, (p_n, y_n, \tau)\}$. For n samples, the cardinality of each confusion matrix set is then computed as:

$$|TP| = \sum_{i=1}^n tp(p_i, y_i, \tau) \quad |FN| = \sum_{i=1}^n fn(p_i, y_i, \tau) \quad |FP| = \sum_{i=1}^n fp(p_i, y_i, \tau) \quad |TN| = \sum_{i=1}^n tn(p_i, y_i, \tau)$$

Common classification metrics are based on these cardinalities. For example, Precision = $|TP| / (|TP| + |FP|)$ is the proportion of positive results that are true positive results. Recall = $|TP| / (|TP| + |FN|)$ indicates the proportion of positives that are correctly identified. These two metrics represent a trade-off between classifier objectives; it is generally undesirable to optimize or evaluate for one while ignoring the other [14]. This makes summary evaluation metrics that balance between these trade-offs popular. Commonly used metrics include:

$$\text{Accuracy} = \frac{|TP| + |TN|}{|TP| + |TN| + |FP| + |FN|} \quad F_1\text{-Score} = \frac{2}{\text{precision}^{-1} + \text{recall}^{-1}} \quad (2)$$

Accuracy is the rate of correct predictions to all predictions. F_1 -Score is a specific instance of F_β -Score = $(1 + \beta^2) \cdot (\text{precision} \cdot \text{recall}) / (\beta^2 \cdot \text{precision} + \text{recall})$, the weighted harmonic mean of precision and recall. The value β indicates recall is considered β times more important than precision.

¹Source code will be made public upon acceptance.

Some metrics like F_β -Score are usually computed at a specific threshold τ whereas others are computed over a range of τ values. For example, the area under the receiver operating characteristic curve (AUROC) is a commonly used ranking performance measure defined in terms of the true positive rate (TPR) and false positive rate (FPR) functions: $\text{AUROC} = \int_{\tau=0}^1 \text{TPR}(\text{FPR}^{-1}(\tau)) d\tau$.

While metrics that rely on confusion matrix set values are commonly used for evaluation, it is hard to use them as a loss during training. These metrics rely on the Heaviside step function, the derivative of which is undefined at the threshold τ and zero everywhere else (Fig. 1, left). This means that these metrics do not have a derivative useful to backpropagate the error through the network during training.

Unfortunately, when a binary classification neural network is trained on a loss function that is different from the evaluation metric, the network is unlikely to optimize for the desired evaluation metric. As shown in our results, when the goal is to balance various confusion matrix set values, e.g., with F_1 -Score, performance is improved by optimizing directly for F_1 -Score instead of the typical binary cross entropy (BCE) loss commonly used for binary classification.

3 Method

We propose a method that aims to unify the training and inference steps of binary neural network classifiers that are evaluated on metrics based on the confusion matrix. Our method has two main steps. First, the Heaviside step function, H , is approximated with a function \mathcal{H} useful for optimization via gradient descent. Then, \mathcal{H} is used to compute a soft version of set membership, which allows for directly optimizing neural network classifiers end-to-end using metrics from the confusion matrix.

We defer the description of the proposed approximations for H to Section 4. The next two sections formally describe soft-set membership and a variety of metrics that, with our method, can be used as losses for training binary neural network classifiers.

Soft set membership: We use soft sets, a generalization of fuzzy sets [26], to directly optimize confusion matrix based metrics. A soft set μ in U , the initial universal set, is defined by the membership function $\mu : U \rightarrow [0, 1]$. For $x \in U$, the set membership function $\mu(x)$ specifies a degree of belonging for x to set u .

In order to compute confusion matrix based metrics, we use the notion of soft sets in place of strict sets. Soft set membership corresponds to the degree to which a sample tuple (p, y, τ) belongs to a confusion matrix set. Formally, we define the soft confusion matrix set membership functions with truth tables for prediction and ground truth pairs (p, y) relative to τ as:

$$\begin{aligned} tp_s(p, y, \tau) &= \begin{cases} \mathcal{H}(p, \tau) & y = 1 \text{ or } p < \tau \\ 1 - \mathcal{H}(p, \tau) & \text{else} \end{cases} & fn_s(p, y, \tau) &= \begin{cases} 1 - \mathcal{H}(p, \tau) & y = 1 \text{ or } p \geq \tau \\ \mathcal{H}(p, \tau) & \text{else} \end{cases} \\ fp_s(p, y, \tau) &= \begin{cases} \mathcal{H}(p, \tau) & y = 0 \text{ or } p < \tau \\ 1 - \mathcal{H}(p, \tau) & \text{else} \end{cases} & tn_s(p, y, \tau) &= \begin{cases} 1 - \mathcal{H}(p, \tau) & y = 0 \text{ or } p \geq \tau \\ \mathcal{H}(p, \tau) & \text{else} \end{cases} \end{aligned} \quad (3)$$

After computing per-sample soft-set values, specific metrics can be approximated by summing over the relevant elements of the confusion matrix. For instance, we approximate precision, $|TP|/(|TP| + |FP|)$, summing over n samples, where $|TP_s| = \sum_{i=1}^n tp_s(p_i, y_i, \tau)$ and $|FP_s| = \sum_{i=1}^n fp_s(p_i, y_i, \tau)$. In practice, this summation occurs at training time over mini-batches while optimizing via gradient descent. Because gradient descent and its variants expect a small but representative sample of the broader data [4], the proposed method also expects a representative sample.

Metrics and losses: Any metric composed of confusion matrix set values (TP , FP , FN , and TN) can be directly optimized using our proposed method. In our experiments, we train and evaluate on Accuracy, F_1 -Score, AUROC, and F_β -Score [34]. We chose these metrics to show the flexibility of our approach. Accuracy, F_1 -Score and F_β -Score may be selected based on class imbalance and resulting tradeoffs. AUROC illustrates that our method can be used even when computation over a range of thresholds, τ , is required. Our experiments demonstrate the efficacy of our method when used to train a classifier with these objective functions and soft set membership (eq. 3).

4 Proposed approximations for the Heaviside step function

Our method requires an approximation, \mathcal{H} , of the Heaviside step function that is compatible with backpropagation. In this section, we formalize desirable properties for the approximation \mathcal{H} . Then, we propose two potential approximations that we later evaluate in our experiments.

Heaviside function approximation properties: A useful approximation would have a non-zero gradient: $\mathcal{H}'(p, \tau) \neq 0, \forall \tau$. This is important to train via backpropagation.

The approximation should also maintain two important properties of the original Heaviside step function, H . First, like H , the approximation should meet the properties of a cumulative distribution function (CDF). That is, the approximation should be right-continuous, be non-decreasing, ensure all outputs are in $[0, 1]$, and follow:

$$\lim_{p \rightarrow 0} \mathcal{H}(p, \tau) = 0 \quad \forall \tau \qquad \lim_{p \rightarrow 1} \mathcal{H}(p, \tau) = 1 \quad \forall \tau \quad (4)$$

The properties above ensure that for a given ground truth label, the sum of the probabilities of the positive and negative predictions is equal to 1.

Second, to remove bias towards one class or the other, the approximation should reflect the fact that a given sample could be a member of either class with equal probability at the threshold $p = \tau$. In the discrete case of H , we choose $H(p = \tau, \tau) = 1$ to ensure right-continuity required by the properties of a CDF. For continuous approximations, $\mathcal{H}(p = \tau, \tau) = 0.5$ is a desirable property.

Sigmoid Heaviside function approximation: One approximation method for H , proposed by [24], is the sigmoid function $s_0(k; p) = (1 + e^{-kp})^{-1}$ (Fig. 1, middle). We reparameterize s_0 to account for τ : $\mathcal{H}^s(k, p, \tau) = (1 + e^{-k(p-\tau)})^{-1}$. We discuss the hyperparameters k and τ in Section 5.

Linear Heaviside function approximation: We propose a novel approximation of H that adheres to the desired properties discussed previously. This approximation, \mathcal{H}^l , is a five-point linearly interpolated function, shown in Figure 1 (right). \mathcal{H}^l is defined over $[0, 1]$ and parameterized by a given threshold τ and a slope parameter δ , which define three linear segments with slopes m_1 , m_2 , and m_3 . The slope of each line segment is:

$$m_1 = \frac{\delta}{\tau - \frac{\tau_m}{2}} \qquad m_2 = \frac{1 - 2\delta}{\tau_m} \qquad m_3 = \frac{\delta}{1 - \tau - \frac{\tau_m}{2}}$$

with $\tau_m = \min\{\tau, 1 - \tau\}$, in order to ensure a gradient suitable for backpropagation. The linear Heaviside approximation is thus given by:

$$\mathcal{H}^l = \begin{cases} p \cdot m_1 & \text{if } p < \tau - \frac{\tau_m}{2} \\ p \cdot m_3 + (1 - \delta - m_3(\tau + \frac{\tau_m}{2})) & \text{if } p > \tau + \frac{\tau_m}{2} \\ p \cdot m_2 + (0.5 - m_2\tau) & \text{otherwise} \end{cases} \quad (5)$$

Considering the threshold τ in the formulation of \mathcal{H}^l ensures $\mathcal{H}^l(p = \tau, \tau) = 0.5$ while maintaining the limits in eq. (4). The derivation of eq. (5) is provided in Section 3 of the supplementary material.

Computational efficiency: At training time, an objective function with our proposed method has a runtime linear with regard to the number of samples. This is a large improvement over adversarial methods such as [11] which have at best cubic runtime. In practice however, optimizing for a metric with \mathcal{H} over all samples in each batch could lead to increased run time due to the number of constant-time operations required to compute the metric. To mitigate this and further minimize run time, we observe that our proposed \mathcal{H} can be replaced with an reasonably-sized $O(1)$ lookup table by truncating p to several decimal places and precomputing \mathcal{H} for values of p and τ over the range $[0, 1]$. For example, if an interval between values of τ is set to 0.1 and p is truncated at two decimal places, the lookup table has only 1,000 elements. Using 8-bit storage, this table consumes 1kB of memory.

5 Experiments

This section presents four experiments to (1) compare the two Heaviside approximations and the effects of different batch sizes on our proposed method, (2) evaluate the performance of our approach against several baselines on tabular data, (3) evaluate the ability of our method to balance precision and recall during training, and (4) evaluate our approach on higher-dimensional image data.

Datasets: Experiments were conducted on two synthetic datasets and five publicly available datasets. The latter datasets, both tabular and higher-dimensional image data, were chosen for their varying

levels of class imbalance as explained later. All datasets were minimally pre-processed and split into separate train, test, and validation sets. See Section 1 of the supplementary material for more details.

Architecture and training: Our experiments aim to fairly evaluate our method using different objective functions. Therefore, the same network architecture and training scheme was used unless otherwise noted. The binary classifier for tabular data was a feedforward neural network consisting of three fully connected layers of 32 units, 16 units, and 1 unit. The first two layers were activated via Rectified Linear Unit (ReLU) [27] and followed by dropout [16]. The final layer was a sigmoid-activated single-unit output. For image datasets, the Tiny YoloV3 [31] architecture was used. The ADAM optimizer [21] was used for training with $lr = 0.001$ and batch size of 1024 for tabular datasets, and $lr = 0.0001$ and batch size of 128 for image datasets. The same batch size and learning rate were used for all methods except [11], which used hyperparameters (e.g., batch size of 20) suggested by the first author through personal communication. Early stopping was used to terminate training after the validation loss stopped decreasing over a sliding window of 100 epochs. Each model optimized via a specific loss was trained using PyTorch or Tensorflow. For tabular data, our method with AUROC and the adversarial baseline [11] were implemented in PyTorch. Models for all other losses on tabular data were implemented in Tensorflow. Also, models for the image datasets were trained using PyTorch. We provide open source implementations of our proposed approach for both deep learning libraries. Training systems used either an NVIDIA Titan X or RTX 2080ti GPU with an Intel i7 3.7GHz processor and 32GB of RAM, with the exception of the adversarial approach to optimize F_1 -Score [11], which had to be run on a CPU due to the author’s provided implementation.

Hyperparameters: Our method introduces two new hyperparameters: τ , and k or δ . We empirically determined values of $\tau = 0.5$, $k = 10$ for \mathcal{H}^s , and $\delta = 0.1$ for \mathcal{H}^l , which were used for all experiments. Given the results of these experiments on a wide range of problems, we believe these values work well in practice and, therefore, do not require extra effort for tuning them.

The incorporation of an approximation for the Heaviside step function introduces the k or δ parameter, depending on which approximation is chosen. For the sigmoid approximation, as k decreases, $\mathcal{H}^{s'}$ becomes smoother, facilitating gradient descent. However, in the limit, the approximation may no longer approach H as discussed in Section 2 of the supplementary material. Similar to the parameter k in the sigmoid approximation, we define a slope parameter, δ , for our proposed \mathcal{H}^l . A larger δ provides a smoother derivative but further deviation from H . However, unlike \mathcal{H}^s , \mathcal{H}^l always approaches H in the limit. Therefore, the particular choice of δ is less crucial within a reasonable range. We empirically determined that $0.1 \leq \delta \leq 0.2$ works well in practice.

Baselines: We trained networks using the typical BCE loss. We also compare against two existing approaches for optimizing specific confusion matrix metrics: an adversarial approach for F_1 -score [11], and using an approximation of the Wilcoxon-Mann-Whitney (WMW) statistic for AUROC [38].

The supplementary material, Section 5.1, provides comparisons with other, less related methods of binary classification. In particular, we compare against neural network classifiers trained on Dice [25], which is designed for image segmentation rather than classification. We also include comparisons with Two-Step EUM from [22] and SVM^{perf} [17], which are not neural network methods.

Other machine learning techniques: Our proposed method is a one-step method and does not incorporate search for an optimal evaluation threshold T given a trained network. However, our method can be used in combination with the plug-in method [28], which empirically searches for an evaluation threshold T on validation data. We demonstrate this possibility in additional results described in Section 5.2 of the supplementary material.

Moreover, our method avoids the need to weight the loss or resample the dataset, techniques commonly used for learning from imbalanced data [14]. However, Section 5.3 in the supplementary material provides comparisons with both weighting and oversampling.

5.1 Batch size and data imbalance

Our first experiment examined how the choice of Heaviside approximation and batch size influence the performance of our method on synthetic datasets with data imbalance. The datasets were generated by creating two isotropic gaussian blobs and removing a randomly-sampled proportion of the positive data points. The synthetic datasets had a positive to negative sample balance of 33% and 4.76%.

Table 1: Losses (rows): Accuracy (Acc), F_1 , and AUROC (ROC) via sigmoid (s) and linear (l) approximation; F_1 -Score \dagger via adversarial approach [11] and AUROC \ddagger via WMW statistic [38]; BCE is traditional binary cross-entropy. Bold indicates performance better than or equal to the BCE baseline. Gray signifies the network is trained and evaluated on different metrics.

		CocktailParty ($\mu \pm \sigma$)			Adult ($\mu \pm \sigma$)		
Loss		Accuracy	F_1 -Score	AUROC	Accuracy	F_1 -Score	AUROC
(1)	Acc^l	0.85 \pm 0.01	0.70 \pm 0.03	0.78 \pm 0.02	0.81 \pm 0.01	0.33 \pm 0.12	0.60 \pm 0.04
(2)	Acc^s	0.85 \pm 0.01	0.71 \pm 0.02	0.78 \pm 0.02	0.81 \pm 0.01	0.33 \pm 0.12	0.60 \pm 0.04
(3)	F_1^l	0.86 \pm 0.01	0.77 \pm 0.02	0.83 \pm 0.01	0.75 \pm 0.05	0.61 \pm 0.03	0.78 \pm 0.02
(4)	F_1^s	0.86 \pm 0.01	0.77 \pm 0.02	0.84 \pm 0.01	0.74 \pm 0.07	0.61 \pm 0.03	0.77 \pm 0.02
(5)	F_1^\dagger	0.76 \pm 0.01	0.29 \pm 0.01	0.59 \pm 0.01	0.79 \pm 0.02	0.21 \pm 0.02	0.56 \pm 0.02
(6)	ROC^l	0.61 \pm 0.01	0.60 \pm 0.01	0.71 \pm 0.01	0.42 \pm 0.02	0.41 \pm 0.02	0.55 \pm 0.02
(7)	ROC^s	0.63 \pm 0.01	0.62 \pm 0.01	0.69 \pm 0.01	0.51 \pm 0.02	0.49 \pm 0.02	0.63 \pm 0.02
(8)	ROC^\ddagger	0.61 \pm 0.20	0.29 \pm 0.29	0.56 \pm 0.12	0.55 \pm 0.26	0.26 \pm 0.19	0.54 \pm 0.08
(9)	BCE	0.83 \pm 0.05	0.71 \pm 0.11	0.79 \pm 0.07	0.75 \pm 0.09	0.30 \pm 0.16	0.60 \pm 0.07

		Mammography ($\mu \pm \sigma$)			Kaggle ($\mu \pm \sigma$)		
Loss		Accuracy	F_1 -Score	AUROC	Accuracy	F_1 -Score	AUROC
(1)	Acc^l	0.98 \pm 0.00	0.00 \pm 0.00	0.50 \pm 0.00	1.00 \pm 0.00	0.09 \pm 0.26	0.54 \pm 0.12
(2)	Acc^s	0.98 \pm 0.00	0.00 \pm 0.00	0.50 \pm 0.00	1.00 \pm 0.00	0.08 \pm 0.25	0.54 \pm 0.12
(3)	F_1^l	0.99 \pm 0.00	0.73 \pm 0.05	0.84 \pm 0.03	1.00 \pm 0.00	0.82 \pm 0.03	0.90 \pm 0.02
(4)	F_1^s	0.99 \pm 0.00	0.70 \pm 0.04	0.84 \pm 0.03	1.00 \pm 0.00	0.81 \pm 0.03	0.89 \pm 0.02
(5)	F_1^\dagger	0.99 \pm 0.03	0.60 \pm 0.03	0.73 \pm 0.03	1.00 \pm 0.02	0.75 \pm 0.02	0.82 \pm 0.02
(6)	ROC^l	0.55 \pm 0.03	0.17 \pm 0.03	0.72 \pm 0.03	0.39 \pm 0.02	0.16 \pm 0.02	0.66 \pm 0.02
(7)	ROC^s	0.55 \pm 0.03	0.34 \pm 0.03	0.71 \pm 0.03	0.48 \pm 0.02	0.37 \pm 0.02	0.70 \pm 0.02
(8)	ROC^\ddagger	0.53 \pm 0.46	0.18 \pm 0.21	0.61 \pm 0.16	0.82 \pm 0.35	0.34 \pm 0.32	0.75 \pm 0.18
(9)	BCE	0.98 \pm 0.00	0.58 \pm 0.18	0.75 \pm 0.10	1.00 \pm 0.00	0.65 \pm 0.27	0.79 \pm 0.14

We trained and evaluated models on Accuracy and F_1 -Score by directly optimizing for the respective metric over 10 trials. We used the sigmoid and the piecewise linear Heaviside approximations, and considered batch sizes in $\{128, 1024, 2048, 4096\}$.

Training batch size had a minimal effect on final classifier performance in our experiments and the impact of the choice of approximation varied with class imbalance. The performance of \mathcal{H}^l and \mathcal{H}^s were similar for the more balanced dataset (Synthetic 33%). However, in the case of imbalanced data (Synthetic 5%) and batch sizes $\{1024, 2048\}$, the performance of the \mathcal{H}^l was greater than of \mathcal{H}^s for the F_1 loss and F_1 -Score evaluation metric. For Accuracy loss, performance evaluated on F_1 -Score was zero, due to the network’s incentive to maximize Accuracy by predicting only dominant-class samples [14]. We believe that the advantage of the \mathcal{H}^l in some cases is due to its adherence to the key properties mentioned in Section 4. Detailed results, including the BCE baseline, are provided in Section 4.1 of the supplementary material. Our method is comparable with or better than BCE.

For the following experiments on tabular data, we chose a batch size of 1024. Further analysis supporting this decision with a real-world dataset is in Section 4.2 of the supplementary material.

5.2 Direct optimization of metrics on tabular data

We evaluate our proposed approach using four tabular datasets with different levels of class imbalance. The CocktailParty dataset has a 30.29% positive class balance making it the most class-balanced dataset of those considered in this experiment. Salary classification data in the Adult dataset has a 23.93% positive class balance. Classifications of microcalcifications in the Mammography dataset is heavily skewed with a 2.32% positive class balance. Lastly, the Kaggle Credit Card Fraud Detection dataset has the most extreme class balance with only a 0.17% positive class balance.

We compare the performance of neural networks trained to directly optimize F_1 -Score, Accuracy, and AUROC with our proposed method against baseline approaches. The baselines in this experiment were neural-network methods that optimize BCE loss and two approaches for optimizing specific metrics: an adversarial approach for F_1 -score by [11], and an approximation of the WMW statistic

Table 2: **Mammography** ($\mu \pm \sigma$) dataset: F_β ($\beta = \{1, 2, 3\}$) loss via our method, with the *linear* or *sigmoid* approximation, to balance between precision and recall while maximizing F_1 -Score.

Loss	F_1 -Score		Precision		Recall	
	<i>linear</i>	<i>sigmoid</i>	<i>linear</i>	<i>sigmoid</i>	<i>linear</i>	<i>sigmoid</i>
F_1	0.729 ± 0.05	0.700 ± 0.04	0.776 ± 0.06	0.717 ± 0.07	0.692 ± 0.07	0.694 ± 0.07
F_2	0.652 ± 0.04	0.648 ± 0.06	0.600 ± 0.07	0.566 ± 0.08	0.729 ± 0.07	$0.770 \pm 0.07s$
F_3	0.602 ± 0.04	0.616 ± 0.07	0.487 ± 0.04	0.507 ± 0.08	0.793 ± 0.05	0.794 ± 0.06

for AUROC per [38]. We provide additional comparisons with less directly related methods of binary classification in Section 5.1 of the supplementary material.

Performance of the networks was evaluated on F_1 -Score, Accuracy, and AUROC over 10 repeated trials to control for the effects of random weight initialization. We report the mean of results evaluated over threshold values $T = \{0.1, 0.2, \dots, 0.9\}$ across all trials. Note that in comparison to [11], the adversarial approach did not perform as well in our experiments. We used a PyTorch implementation provided by the author, but [11] utilized an implementation in Julia and Flux ML, which could explain the difference.

We examined networks trained via our method with the three evaluation metrics (Table 1) and found:

Optimizing for F_1 Score. Our method of direct optimization of F_1 -Score with either the linear or sigmoid Heaviside approximation outperforms baselines when evaluated on F_1 -Score for all datasets. In Table 1, lines (3) and (4) have higher F_1 -Score than lines (5) and (9). Additionally, when evaluated on Accuracy and AUROC, networks trained with our method of direct optimization of F_1 -Score almost always outperform the baseline—the exception being the Adult dataset evaluated on Accuracy.

Optimizing for Accuracy. For the two more balanced datasets, the networks trained with our method for direct optimization of Accuracy outperform the BCE baseline when evaluated on Accuracy. In Table 1, lines (1) and (2) have higher Accuracy than line (9) for CocktailParty and Adult datasets. The more imbalanced datasets, Mammography and Kaggle, show limitations of the Accuracy metric due to its propensity to predict only dominant-class examples [14]. For all datasets, training on F_1 -Score results in better performance than training on Accuracy when evaluated on F_1 -Score or AUROC.

Optimizing for AUROC. Neither our method of directly optimizing AUROC nor optimizing AUROC via the WCW statistic [38] consistently outperform traditional BCE. In Table 1, lines (6), (7), and (8) have lower F_1 -Score, Accuracy, and AUROC than line (9) except for one exception. This may be due in part to the AUROC metric’s challenge with scale assumptions [12]. Moreover, an unbiased estimator of gradient direction is not available in the case of AUROC [1], which may also contribute to lackluster performance. However, for the Adult dataset, AUROC optimized via our method outperforms traditional BCE and AUROC optimized via the WMW statistic [38].

5.3 Balancing between precision and recall

Our method also allows training-time optimization that balances between precision and recall using F_β -Score. This end-to-end approach to training is particularly useful in real-world scenarios where there is a high cost associated with missed detections.

Results in Table 2 show that directly optimizing F_β -Score is an effective way of maintaining maximum classifier performance measured via F_1 -Score, while balancing between precision and recall at a ratio appropriate for a given task. Increasing values of β correspond to an increased preference toward recall with small loss of total performance measured by F_1 -Score. Similar results on optimizing for F_β -Score with additional datasets are provided in Section 6 of the supplementary material.

5.4 Direct optimization of metrics on image data

We conducted experiments similar to the those in Section 5.2 with higher dimensional data using two different binary image datasets created from the CIFAR-10 dataset [23]. The CIFAR-10-Transportation and CIFAR-10-Frog datasets had a 40% and 10% positive class balance, respectively.

Table 3: Losses (rows): Accuracy (Acc) and F_1 via linear (l) and sigmoid (s) approximation; BCE is traditional binary cross-entropy. Bold indicates performance better than or equal to BCE baseline. Gray signifies the network is trained and evaluated on different metrics.

CIFAR-10-Transportation Results ($\mu \pm \sigma$)				CIFAR-10-Frog Results ($\mu \pm \sigma$)			
	<i>Loss</i>	Accuracy	F_1 -Score		<i>Loss</i>	Accuracy	F_1 -Score
(1)	Acc^l	0.921 \pm 0.00	0.900 \pm 0.00	(1)	Acc^l	0.911 \pm 0.01	0.407 \pm 0.11
(2)	Acc^s	0.921 \pm 0.01	0.901 \pm 0.01	(2)	Acc^s	0.909 \pm 0.01	0.377 \pm 0.14
(3)	F_1^l	0.927 \pm 0.01	0.909 \pm 0.01	(3)	F_1^l	0.947 \pm 0.00	0.729 \pm 0.01
(4)	F_1^s	0.931 \pm 0.00	0.914 \pm 0.01	(4)	F_1^s	0.948 \pm 0.00	0.740 \pm 0.01
(5)	<i>BCE</i>	0.909 \pm 0.00	0.882 \pm 0.00	(5)	<i>BCE</i>	0.935 \pm 0.00	0.601 \pm 0.05

Given limitations with AUROC found in earlier experiments, we focused on Accuracy and F_1 -Score. We also excluded the adversarial approach to optimize F_1 -Score [11] due to long runtime on tabular data. As a reference, training networks for the tabular datasets on F_1 -Score using our method on a CPU took a median time of 2.3 ± 0.16 minutes. Training with the adversarial approach on the same CPU took a median time of 70 ± 118 minutes. Otherwise, we use the same set up from Section 5.2.

Overall, our findings with image data in Table 3 are consistent with tabular results from Section 5.2:

Optimizing for F_1 Score. Networks trained with our method to directly optimize F_1 -Score outperform traditional BCE for both datasets when evaluated on both Accuracy and F_1 -Score. In Table 3, lines (3) and (4) have higher Accuracy and F_1 -Score than line (5).

Optimizing for Accuracy. The results for our method directly optimizing Accuracy (lines (1) and (2) in Table 3) and results for BCE (line (5) in Table 3) are similar. There is a slight advantage for our method with the more balanced dataset of transportation images, and a slight advantage for BCE with the less balanced dataset of frog images. Consistent with the Mammography and Kaggle results in Table 1, in the case of class imbalance, it is not best to directly optimize the Accuracy during training because optimizing for F_1 -Score leads to higher values for the Accuracy evaluation metric.

Section 5.4 of the supplementary material includes results for neural networks trained with the Dice coefficient [25] as the objective function. We compare against Dice because it is a different approach to reformulating a similar type of metric for use as an objective function. Our method outperforms Dice, likely because Dice was intended for image segmentation, not image classification.

6 Related work

This approach takes the viewpoint on performance metrics that [7] called Population Utility (PU) and [39] referred to as empirical utility maximization (EUM). Our method aims to learn a classifier with optimal performance on training data.

Our work is inspired by research on the direct optimization of evaluation metrics for binary classification. This includes plug-in methods that empirically estimate a threshold for a classifier on a metric. For example, [28] demonstrated the applicability of plug-in classifiers to optimize F_1 -Score with linear models. For metrics based on linear combinations of confusion matrix set cardinalities, [22] identified an optimal plug-in classifier with a metric-dependent threshold. Also, [20] explored the Precision@K metric for linear models in the context of ranking. Our approach is not a competitor to plug-in methods, but rather an approach to train a neural network classifier directly on a metric based on the confusion matrix. As such, it could be used in conjunction with a plug-in method, if desired, as shown in Section 5.2 in the supplementary material.

Works such as [5, 19] optimized specific metrics like Precision@K and F_1 -Score in online learning, characterized by the sequential availability of data. Our work does not address online learning, but batch methods. Additionally, other work has focused on optimizing AUROC [15, 38], F-score [8, 40], and AUPRC in the context of ranking [10]. [1] discusses the class of “linear-fractional” metrics such as F-score. We compare against [38]’s method of optimizing AUROC, a metric that is not of the “linear-fractional” class. Rather than focusing on a single specific metric, we provide a flexible means for optimizing a neural network using any metric based on confusion matrix sets with minimal reformulation of the objective function and maximal control of the metric during optimization. For

example, our experiments in Section 5.3 show how tradeoffs between precision and recall can be made by adjusting the β parameter of the F_β -score during training with our method.

In the field of computer vision, differentiable surrogate losses have been proposed for the Jaccard Index [2, 30, 33] and Dice score [3, 25, 29, 36], to which we compare in Sections 5.1 and 5.4 of the supplementary material. However these methods use the softmax output of the network, which is different than our proposed approach to utilize an approximation of H and the notion of soft sets.

Recently, adversarial approaches have emerged as another related area of research. [37] used a structured support vector machine and reported performance on Precision@K as well as F_1 -Score. [11], which we compare against, improved performance via a marginalization technique that ensured polynomial time convergence and evaluated on Accuracy and F_1 -Score, among other metrics, while reporting performance relative to BCE. Downsides of the latter approach are that it is limited to a small batch size, on the order of 25 samples, and has cubic runtime complexity.

A parallel line of work focused on dealing with class imbalance by dropping data in the over-represented class or augmenting the under-represented data by synthesizing new samples. In regards to this re-sampling approach, [9] found under-sampling preferential to over-sampling. However, in both cases it was vital to maintain representative distributions for both the over and under-represented classes [14]. Therefore, strategic approaches toward handling imbalance via data preprocessing have been proposed, including the Synthetic Minority Over-sampling Technique (SMOTE) [6]. Interestingly, recent work has found re-sampling based approaches inadequate and suggests a larger number of samples is necessary to improve results [18]. As an alternative to re-sampling, our work focuses on choosing an appropriate evaluation metric for the given level of class imbalance and directly optimizing this metric as a loss. Nonetheless, to illustrate that our proposed approach can be combined with other machine learning techniques, we provide results combining our method with both weighting and oversampling in Section 5.3 of the supplementary material.

7 Conclusion

We proposed a novel method to directly optimize confusion matrix based metrics using a Heaviside function approximation and soft set membership. Our method links the training and inference steps, making our approach end-to-end. Our proposed method is unique in its flexibility as it allows for optimization of any metric based on confusion matrix sets. Our method can also be combined with other machine learning techniques, such as plug-in methods, weighting, and oversampling.

We evaluate two approximations of H , and illustrate that our novel linear approximation more broadly facilitates the use of our method with its behavior at the limits in comparison to a sigmoid approximation. We also provide practical implications about batch size when optimizing confusion matrix based metrics.

Our experiments showed the efficacy of the proposed approach in training end-to-end binary classifiers compared to other methods of direct metric optimization as well as against the traditional BCE loss when optimizing for F_1 -Score. In all cases, our method outperformed the baseline approaches that directly optimize F_1 -Score [11], which had much longer training time, and AUROC [38], which was designed for the specific metric. Our experiments also revealed cases where optimizing the evaluation metric as a loss is not preferable to some surrogate — challenging a common assumption. In the future, we are interested in further studying the implications of this finding on choosing evaluation metrics, especially in the case of class imbalance, which is common in the real world [32].

References

- [1] Han Bao and Masashi Sugiyama. Calibrated surrogate maximization of linear-fractional utility in binary classification. In *International Conference on Artificial Intelligence and Statistics*, 2020.
- [2] Maxim Berman, Amal Rannen Triki, and Matthew B Blaschko. The lovász-softmax loss: A tractable surrogate for the optimization of the intersection-over-union measure in neural networks. In *Proceedings of the IEEE Conference on Computer Vision and Pattern Recognition*, pages 4413–4421, 2018.

- [3] Jeroen Bertels, Tom Eelbode, Maxim Berman, Dirk Vandermeulen, Frederik Maes, Raf Bisschops, and Matthew B Blaschko. Optimizing the dice score and jaccard index for medical image segmentation: Theory and practice. In *International Conference on Medical Image Computing and Computer-Assisted Intervention*, 2019.
- [4] Léon Bottou. Stochastic gradient descent tricks. In *Neural networks: Tricks of the trade*, pages 421–436. Springer, 2012.
- [5] Róbert Busa-Fekete, Balázs Szörényi, Krzysztof Dembczynski, and Eyke Hüllermeier. Online f-measure optimization. In *NeurIPS*, pages 595–603, 2015.
- [6] Nitesh V Chawla, Kevin W Bowyer, Lawrence O Hall, and W Philip Kegelmeyer. Smote: synthetic minority over-sampling technique. *JAIR*, 16:321–357, 2002.
- [7] Krzysztof Dembczyński, Wojciech Kotłowski, Oluwasanmi Koyejo, and Nagarajan Natarajan. Consistency analysis for binary classification revisited. In *International Conference on Machine Learning*, pages 961–969. PMLR, 2017.
- [8] Krzysztof J Dembczynski, Willem Waegeman, Weiwei Cheng, and Eyke Hüllermeier. An exact algorithm for f-measure maximization. In *NeurIPS*, 2011.
- [9] Chris Drummond and Robert C Holte. C4. 5, class imbalance, and cost sensitivity: why under-sampling beats over-sampling. In *Workshop on learning from imbalanced datasets II*, volume 11, pages 1–8, 2003.
- [10] Elad Eban, Mariano Schain, Alan Mackey, Ariel Gordon, Ryan Rifkin, and Gal Elidan. Scalable Learning of Non-Decomposable Objectives. In *AISTATS*, 2017.
- [11] Rizal Fathony and Zico Kolter. Ap-perf: Incorporating generic performance metrics in differentiable learning. In *AISTATS*, pages 4130–4140, 2020.
- [12] Peter Flach and Meelis Kull. Precision-recall-gain curves: Pr analysis done right. In *NeurIPS*, pages 838–846, 2015.
- [13] Ian Goodfellow, Yoshua Bengio, Aaron Courville, and Yoshua Bengio. *Deep learning*. MIT press Cambridge, 2016.
- [14] Haibo He and Eduardo A Garcia. Learning from imbalanced data. *TKDE*, 21(9):1263–1284, 2009.
- [15] Alan Herschtal and Bhavani Raskutti. Optimising area under the roc curve using gradient descent. In *ICML*, page 49, 2004.
- [16] Geoffrey E. Hinton, Nitish Srivastava, Alex Krizhevsky, Ilya Sutskever, and Ruslan R. Salakhutdinov. Improving neural networks by preventing co-adaptation of feature detectors. *CoRR*, 2012.
- [17] Thorsten Joachims. Training linear svms in linear time. In *Proceedings of the 12th ACM SIGKDD international conference on Knowledge discovery and data mining*, pages 217–226, 2006.
- [18] Brendan Juba and Hai S Le. Precision-recall versus accuracy and the role of large data sets. In *AAAI*, volume 33, pages 4039–4048, 2019.
- [19] Purushottam Kar, Harikrishna Narasimhan, and Prateek Jain. Online and stochastic gradient methods for non-decomposable loss functions. In *NeurIPS*, pages 694–702, 2014.
- [20] Purushottam Kar, Harikrishna Narasimhan, and Prateek Jain. Surrogate functions for maximizing precision at the top. In *ICML*, pages 189–198, 2015.
- [21] Diederik P. Kingma and Jimmy Ba. Adam: A method for stochastic optimization. In Yoshua Bengio and Yann LeCun, editors, *ICLR*, 2015.
- [22] Oluwasanmi O Koyejo, Nagarajan Natarajan, Pradeep K Ravikumar, and Inderjit S Dhillon. Consistent binary classification with generalized performance metrics. In *NeurIPS*, pages 2744–2752, 2014.
- [23] A. Krizhevsky and G. Hinton. Learning multiple layers of features from tiny images. *Master’s thesis, Department of Computer Science, University of Toronto*, 2009.
- [24] Nikolay Kyurkchiev and Svetoslav Markov. Sigmoid functions: some approximation and modelling aspects. *LAP LAMBERT Academic Publishing, Saarbrücken*, 2015.

- [25] Fausto Milletari, Nassir Navab, and Seyed-Ahmad Ahmadi. V-net: Fully convolutional neural networks for volumetric medical image segmentation. In *2016 fourth international conference on 3D vision (3DV)*, 2016.
- [26] Dmitriy Molodtsov. Soft set theory—first results. *CAMWA*, 1999.
- [27] Vinod Nair and Geoffrey E Hinton. Rectified linear units improve restricted boltzmann machines. In *ICML*, pages 807–814, 2010.
- [28] Harikrishna Narasimhan, Rohit Vaish, and Shivani Agarwal. On the statistical consistency of plug-in classifiers for non-decomposable performance measures. In *NeurIPS*, pages 1493–1501, 2014.
- [29] Marcus Nordström, Han Bao, Fredrik Löfman, Henrik Hult, Atsuto Maki, and Masashi Sugiyama. Calibrated surrogate maximization of dice. In *International Conference on Medical Image Computing and Computer-Assisted Intervention*, pages 269–278. Springer, 2020.
- [30] Md Atiqur Rahman and Yang Wang. Optimizing intersection-over-union in deep neural networks for image segmentation. In *International symposium on visual computing*, pages 234–244. Springer, 2016.
- [31] Joseph Redmon and Ali Farhadi. Yolov3: An incremental improvement. *CoRR*, abs/1804.02767, 2018.
- [32] William J Reed. The pareto, zipf and other power laws. *Economics letters*, 74(1):15–19, 2001.
- [33] Hamid Rezaatofghi, Nathan Tsoi, JunYoung Gwak, Amir Sadeghian, Ian Reid, and Silvio Savarese. Generalized intersection over union: A metric and a loss for bounding box regression. In *Proceedings of the IEEE/CVF Conference on Computer Vision and Pattern Recognition*, 2019.
- [34] C. J. Van Rijsbergen. *Information Retrieval*. Butterworth-Heinemann, USA, 2nd edition, 1979.
- [35] Yang Song, Alexander Schwing, Raquel Urtasun, et al. Training deep neural networks via direct loss minimization. In *ICML*, pages 2169–2177, 2016.
- [36] Carole H Sudre, Wenqi Li, Tom Vercauteren, Sebastien Ourselin, and M Jorge Cardoso. Generalised dice overlap as a deep learning loss function for highly unbalanced segmentations. In *Deep learning in medical image analysis and multimodal learning for clinical decision support*, pages 240–248. Springer, 2017.
- [37] Hong Wang, Wei Xing, Kaiser Asif, and Brian Ziebart. Adversarial prediction games for multivariate losses. In *NeurIPS*, pages 2728–2736, 2015.
- [38] Lian Yan, Robert H Dodier, Michael Mozer, and Richard H Wolniewicz. Optimizing classifier performance via an approximation to the wilcoxon-mann-whitney statistic. In *ICML*, 2003.
- [39] Nan Ye, Kian Ming Chai, Wee Sun Lee, and Hai Leong Chieu. Optimizing f-measures: a tale of two approaches. In *Proceedings of the 29th International Conference on Machine Learning*, pages 289–296. Omnipress, 2012.
- [40] Ming-Jie Zhao, Narayanan Edakunni, Adam Pocock, and Gavin Brown. Beyond fano’s inequality: bounds on the optimal f-score, ber, and cost-sensitive risk and their implications. *JMLR*, 2013.

Supplementary Material

An End-to-End Approach for Training Neural Network Binary Classifiers on Metrics Based on the Confusion Matrix

Nathan Tsoi, Kate Candon, Yofiti Milkessa, Marynel Vázquez
Yale University, New Haven, CT 06511
nathan.tsoi@yale.edu

1 Datasets

We report results for experiments on four binary classification datasets of tabular data with varying levels of class imbalance applicable to a wide range of domains (Sec. 5.2 in the paper). We also report results for experiments on two different binary classification datasets created from a commonly used image dataset (Sec. 5.4 in the paper).

For tabular datasets, features were centered and scaled to unit variance, and the data was split into separate train (64%), test (20%) and validation (16%) sets. For image datasets, the data was normalized and split into separate train (67%), test (17%), and validation (17%) sets.

1.1 CocktailParty Dataset

The CocktailParty Dataset¹ [9] consists of annotations for the locations and orientations of six people in a physical space. The task is to predict whether or not two individuals are part of the same conversational group. We use a total of 22 spatial properties describing the locations and orientations of the two individuals as well as those of the other four individuals around them. These features were extracted for every pair of individuals in every frame of the original dataset, resulting in 4800 samples being obtained from 320 frames (320×15 possible pairings = 4800 data points). The spatial coordinates of each data point were chosen such that the individuals in the pair lie along the x-axis with the origin halfway between them. The final dataset has a 30.29% positive class balance.

1.2 Adult Data Set

The Adult Data Set² from the UCI Machine Learning Repository [1] consists of data extracted from the 1994 Census database with the intended task of predicting whether a person makes more than \$50K per year. This dataset has 14 features of which 1 feature, indicating the number of people represented by the data point, was removed as it has no bearing on the labeled outcome. This dataset contains 48842 points of which 11687 are positive resulting in a 23.93% positive class balance.

1.3 Mammography dataset

The binary classification data for microcalcifications in the Mammography dataset [8], available from OpenML,³ is composed of 6 features, all of which were considered in our experiments. This dataset has 11183 total samples, 260 of which are positive making it imbalanced. The dataset has only 2.32% positive-class examples.

¹<https://tev.fbk.eu/technologies/cocktailparty-dataset-multi-view-dataset-social-behavior-analysis>

²<https://archive.ics.uci.edu/ml/machine-learning-databases/adult/>

³<https://www.openml.org/d/310>

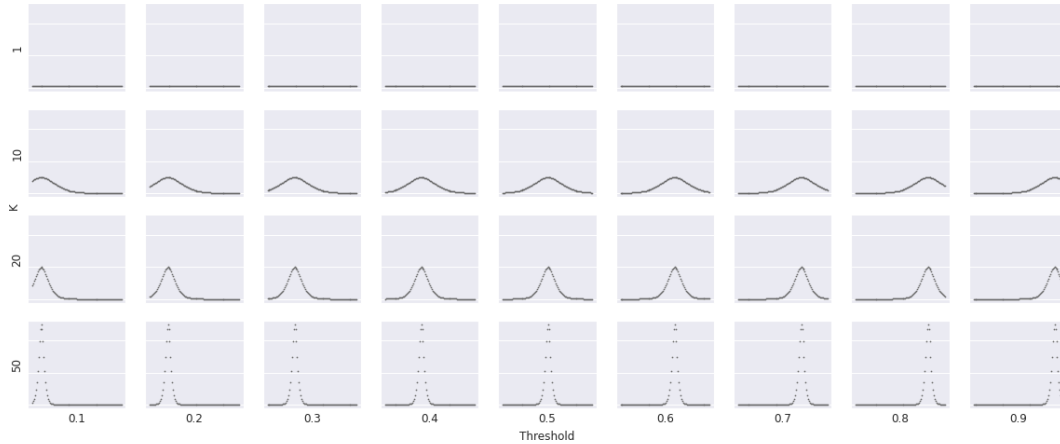


Figure 1: Derivative of the sigmoid approximation of the Heaviside step function by k and τ . As k increases, the range of values with zero gradient increases.

1.4 Kaggle Credit Card Fraud Detection

The Kaggle Credit Card Fraud Detection dataset⁴ consists of transaction data for European card users over two days in September of 2013. It has data for 284807 total transactions and 492 instances of fraud. These positive samples, corresponding to cases of fraud, result in a 0.17% positive-sample balance. The Kaggle dataset has 28 unnamed features as well as two more named features: transaction time and amount. The time feature was removed to avoid learning correlation between time step and label. Amount was log-scaled due to the wide range in values resulting in a total of 29 features.

1.5 Image Datasets

The CIFAR-10 dataset⁵ [4] contains sixty thousand images evenly distributed across ten mutually exclusive classes: airplane, automobile, bird, cat, deer, dog, frog, horse, ship, and truck. Each image is a three-channel color (RGB) image with a size of 32x32 pixels. We created two binary datasets from CIFAR-10, discussed below.

CIFAR-10-Transportation: CIFAR-10-Transportation was created to achieve 40% class balance. If the image was labeled as an airplane, automobile, ship, or truck, it was considered to be in the positive class.

CIFAR-10-Frog: CIFAR-10-Frog was created to achieve 10% class balance. Only images labeled as a frog were considered the positive class.

2 Sigmoid Heaviside function approximation

2.1 Visual analysis of trade-offs when searching for optimal k

As described in Section 4.2 of the paper, a tradeoff must be made when choosing an appropriate value for k in the sigmoid approximation. As k increases, the range of values with zero gradient increases, as shown in Figure 1. However, as k increases, the approximation becomes closer to the Heaviside step function when $\tau = 0.5$, as shown in Figure 2.

It is important to note that for soft-set membership calculation, as k decreases, the number of τ values over which the approximation diverges from the Heaviside step function at the limit increases. In

⁴<https://www.kaggle.com/mlg-ulb/creditcardfraud>

⁵<https://www.cs.toronto.edu/~kriz/cifar.html>

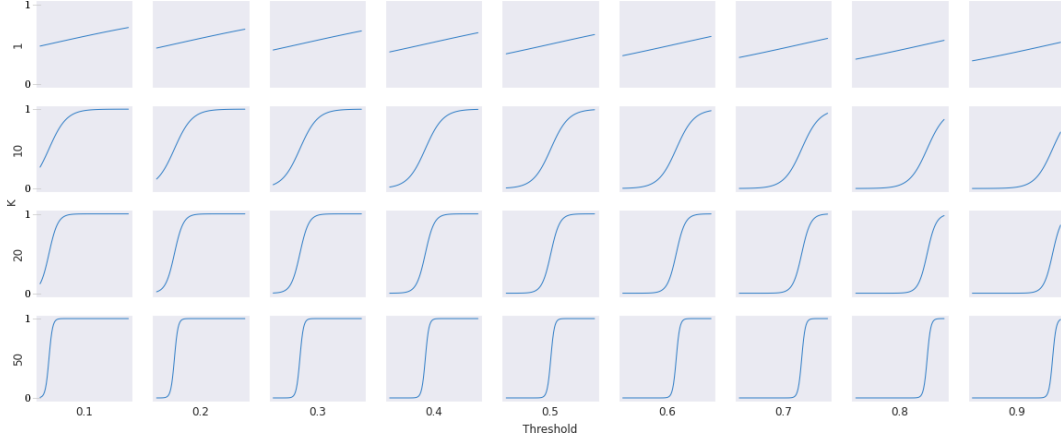


Figure 2: Sigmoid approximation of the Heaviside step function by k and τ . With increased values of k , the approximation becomes closer to the Heaviside step function. As k decreases, the number τ values over which the approximation diverges from the Heaviside step function at the limit increases.

other words, as k decreases, the number of τ values increases for which the sigmoid approximation does not adhere to the following limits:

$$\lim_{p \rightarrow 0} \mathcal{H}(p, \tau) = 0 \quad \forall \tau \quad \lim_{p \rightarrow 1} \mathcal{H}(p, \tau) = 1 \quad \forall \tau \quad (1)$$

Figure 2 illustrates that for $k = 50$, the approximation does approach the limits in Equation 1 for $\tau = \{0.1, 0.2, \dots, 0.9\}$. For $k=1$, the approximation does not approach the limits in Equation 1 for any values of τ .

We searched for the best value of k in $\{1, 10, 20, 50\}$ and found that $k = 10$ led to the best performance.

3 Linear Heaviside function approximation

3.1 Derivation of the linear Heaviside approximation

Our proposed linear Heaviside approximation is formulated to ensure adherence to the properties described in Section 4.1 of the main paper.

We concern ourselves with only the range over $[0,1]$ since we expect the the input to represent a probability in $[0,1]$.

For $0 \leq p \leq 1$, we start by specifying the endpoints to ensure Eq. 1 above, and we define the point at $p = \tau$ to ensure the property $\mathcal{H}(p = \tau, \tau) = 0.5$:

$$\mathcal{H}(p, \tau) = \begin{cases} 0 & \text{if } p = 0 \\ 1 & \text{if } p = 1 \\ 0.5 & \text{if } p = \tau \end{cases} \quad (2)$$

A natural next step would be to solve for a three point linearly interpolated function using the points defined in Eq. 2. However, we find that in practice this is difficult to optimize, perhaps due to the fact that the gradient of one segment becomes much greater than the other as τ approaches 0 or 1. Thus we instead define two more points relative to τ with the introduction of the parameter δ , which makes optimization via backpropagation more stable. We specify these two points to be equal to δ and $1 - \delta$ when the inputs are halfway the distance between τ and the nearest endpoint (0 or 1).

Let τ_m be the distance between τ and the nearest endpoint of \mathcal{H} :

$$\tau_m = \min\{\tau, 1 - \tau\} \quad (3)$$

Then, we define the two new points at which $\mathcal{H}(p, \tau)$ is defined as:

$$\mathcal{H}(p, \tau) = \begin{cases} \delta & \text{if } p = \tau - \frac{\tau_m}{2} \\ 1 - \delta & \text{if } p = \tau + \frac{\tau_m}{2} \end{cases} \quad (4)$$

The parameter δ is chosen such that the function remains non-decreasing, limiting its range to $[0, 0.5]$. Note that, as shown in Figure 3 (left), a choice of $\delta = 0$ would result in gradient equal to zero between $p = 0$ and $p = \tau - \frac{\tau_m}{2}$, as well as between $p = \tau + \frac{\tau_m}{2}$ and $p = 1$. As shown in Figure 3 (middle), a choice of $\delta = 0.5$ would result in a gradient equal to zero between $p = \tau - \frac{\tau_m}{2}$ and $p = \tau + \frac{\tau_m}{2}$. We empirically determined that a value in the range of $0.1 \leq \delta \leq 0.2$ works well. A linear approximation with $\delta = 0.1$ is shown in Figure 3 (right).

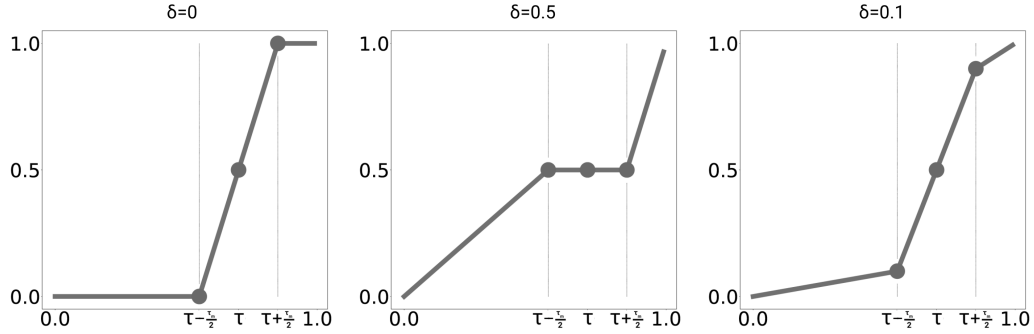


Figure 3: Linear Heaviside approximation \mathcal{H}^l with δ values of 0 (left), 0.5 (middle), and 0.1 (right).

In total, the following five points for \mathcal{H}^l have now been defined as follows:

$$\mathcal{H}(p, \tau) = \begin{cases} 0 & \text{if } p = 0 \\ \delta & \text{if } p = \tau - \frac{\tau_m}{2} \\ 0.5 & \text{if } p = \tau \\ 1 - \delta & \text{if } p = \tau + \frac{\tau_m}{2} \\ 1 & \text{if } p = 1 \end{cases} \quad (5)$$

The property of $\mathcal{H}(p = \tau, \tau) = 0.5$ is now satisfied by our formulation. We can use the points to solve for three line segments that fully define \mathcal{H}^l . We denote the slope and intercept of each segment from left to right as m_1, m_2, m_3 and b_1, b_2, b_3 respectively. These slopes, from left to right, are:

$$m_1 = \frac{\delta}{\tau - \frac{\tau_m}{2}} \quad m_2 = \frac{1 - 2\delta}{\tau_m} \quad m_3 = \frac{\delta}{1 - \tau - \frac{\tau_m}{2}}$$

We can solve for the first intercept, b_1 , with $p = \tau - \frac{\tau_m}{2}$:

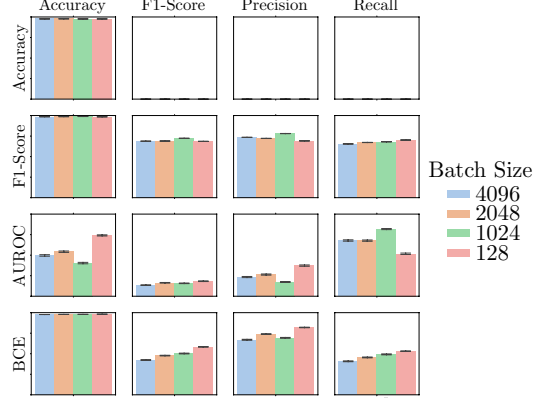


Figure 4: Comparison of batch sizes across objective functions (rows) and metrics (columns). Bar height corresponds to the score. Empty cells indicate zero performance for the Accuracy objective.

$$\begin{aligned}\delta &= m_1\left(\tau - \frac{\tau_m}{2}\right) + b_1 \\ b_1 &= \delta - \left(\frac{\delta}{\tau - \frac{\tau_m}{2}}\right)\left(\tau - \frac{\tau_m}{2}\right) \\ b_1 &= 0\end{aligned}$$

We then solve for the second intercept, b_2 , with $p = \tau$:

$$\begin{aligned}0.5 &= m_2\tau + b_2 \\ b_2 &= 0.5 - m_2\tau\end{aligned}$$

Finally, we solve for the third intercept, b_3 , with $p = \tau + \frac{\tau_m}{2}$:

$$\begin{aligned}1 - \delta &= m_3\left(\tau + \frac{\tau_m}{2}\right) + b_3 \\ b_3 &= 1 - \delta - m_3\left(\tau + \frac{\tau_m}{2}\right)\end{aligned}$$

Therefore the linear approximation is:

$$\mathcal{H}^l = \begin{cases} p \cdot m_1 & \text{if } p < \tau - \frac{\tau_m}{2} \\ p \cdot m_3 + (1 - \delta - m_3(\tau + \frac{\tau_m}{2})) & \text{if } p > \tau + \frac{\tau_m}{2} \\ p \cdot m_2 + (0.5 - m_2\tau) & \text{otherwise} \end{cases} \quad (6)$$

4 Data imbalance results

4.1 Batch size analysis on imbalanced synthetic datasets

The discussion in Section 5.1 of the paper of our experiment on batch size and data imbalance focused on comparing Heaviside approximations. Table 1 provides the results of the experiment, as well as BCE results. Our method is comparable to or better than the BCE baseline.

4.2 Batch size analysis on imbalanced tabular data

Section 5.1 of the paper discusses the effect of batch size on synthetic datasets. In this supplementary experiment, we study the effect of batch size on the Mammography dataset.

Table 1: Accuracy (Acc) and F_1 (F) loss (rows) via sigmoid (s) and linear (l) approximations by batch sizes $\{128, 1024, 2048, 4096\}$. The Synthetic 5% dataset F_1 -Score is zero for Accuracy loss. For both datasets, results are very similar within each metric regardless of batch size and Heaviside approximation. Performance on the Synthetic 5% dataset, F_1^l loss with batch sizes of 1024 and 2048 is comparable, but better than F_1^s .

Synthetic 5% Dataset				
Accuracy ($\mu \pm \sigma$)				
Loss	$B = 128$	1024	2048	4096
Acc^l	0.95 ± 0.01	0.95 ± 0.00	0.95 ± 0.01	0.96 ± 0.01
Acc^s	0.95 ± 0.00	0.95 ± 0.01	0.95 ± 0.00	0.95 ± 0.00
F_1^l	0.89 ± 0.19	0.91 ± 0.15	0.86 ± 0.23	0.83 ± 0.29
F_1^s	0.88 ± 0.20	0.90 ± 0.15	0.79 ± 0.33	0.84 ± 0.27
BCE	0.95 ± 0.02	0.95 ± 0.02	0.95 ± 0.02	0.95 ± 0.02
F_1 -Score ($\mu \pm \sigma$)				
Loss	$B = 128$	1024	2048	4096
Acc^l	0.00 ± 0.00	0.00 ± 0.00	0.00 ± 0.00	0.00 ± 0.00
Acc^s	0.00 ± 0.00	0.00 ± 0.00	0.00 ± 0.00	0.00 ± 0.00
F_1^l	0.42 ± 0.13	0.46 ± 0.12	0.41 ± 0.15	0.38 ± 0.17
F_1^s	0.42 ± 0.15	0.41 ± 0.13	0.34 ± 0.18	0.38 ± 0.18
BCE	0.29 ± 0.19	0.25 ± 0.21	0.26 ± 0.20	0.22 ± 0.20
Synthetic 33% Dataset				
Accuracy ($\mu \pm \sigma$)				
Loss	$B = 128$	1024	2048	4096
Acc^l	0.86 ± 0.01	0.86 ± 0.01	0.85 ± 0.00	0.85 ± 0.01
Acc^s	0.85 ± 0.01	0.85 ± 0.01	0.85 ± 0.01	0.85 ± 0.01
F_1^l	0.85 ± 0.01	0.85 ± 0.01	0.85 ± 0.01	0.85 ± 0.01
F_1^s	0.85 ± 0.01	0.85 ± 0.01	0.85 ± 0.01	0.85 ± 0.01
BCE	0.81 ± 0.05	0.81 ± 0.05	0.81 ± 0.05	0.81 ± 0.05
F_1 -Score ($\mu \pm \sigma$)				
Loss	$B = 128$	1024	2048	4096
Acc^l	0.77 ± 0.01	0.78 ± 0.01	0.77 ± 0.01	0.77 ± 0.02
Acc^s	0.77 ± 0.01	0.78 ± 0.01	0.77 ± 0.02	0.77 ± 0.02
F_1^l	0.77 ± 0.01	0.79 ± 0.01	0.79 ± 0.01	0.78 ± 0.01
F_1^s	0.78 ± 0.01	0.78 ± 0.01	0.78 ± 0.01	0.78 ± 0.01
BCE	0.69 ± 0.10	0.69 ± 0.10	0.69 ± 0.10	0.69 ± 0.11

Table 2: Absolute difference between batch F_1 -Score and the F_1 -Score of the Mammography dataset by batch size B . See the text for details.

$B = 128$	$B = 1024$	$B = 2048$	$B = 4096$
0.041 ± 0.23	0.005 ± 0.06	0.009 ± 0.05	0.006 ± 0.03

Throughout training, F_1 -Score was computed against both the current batch of the train split as well as the entire dataset using the network undergoing training. The difference between the batch F_1 -Score and the F_1 -Score of the entire dataset was then aggregated. We performed this test for batch sizes of $\{128, 1024, 2048, 4096\}$ samples, which corresponds to $\{1\%, 9\%, 18\%, 37\%\}$ of the total samples in the dataset. As can be seen in Table 2, the absolute difference between batch F_1 -Score and total F_1 -Score decreases as the batch size increases. This trend is observed both in terms of absolute mean difference and standard deviation.

The relative performance of classifiers across batch sizes is shown in Figure 4. Directly optimizing Accuracy results in zero precision, recall, and F_1 -Score because all predictions are negative. Training on F_1 -Score, AUROC, and BCE produce non-zero F_1 -Scores that are similar across batch sizes with

Table 3: Other baselines.

		CocktailParty ($\mu \pm \sigma$)			Adult ($\mu \pm \sigma$)		
	Loss	Accuracy	F_1 -Score	AUROC	Accuracy	F_1 -Score	AUROC
(10)	Dice	0.68 ± 0.04	0.49 ± 0.02	0.56 ± 0.02	0.50 ± 0.15	0.40 ± 0.02	0.55 ± 0.02
(11)	EUM	0.78	0.66	0.75	0.55	0.44	0.56
(12)	SVM_E^{perf}	0.82	0.66	0.75	0.81	0.60	0.75
(13)	$SVM_{F_1}^{perf}$	0.78	0.69	0.78	0.51	0.48	0.66
(14)	SVM_{ROC}^{perf}	0.76	0.67	0.77	0.32	0.41	0.56
		Mammography ($\mu \pm \sigma$)			Kaggle ($\mu \pm \sigma$)		
	Loss	Accuracy	F_1 -Score	AUROC	Accuracy	F_1 -Score	AUROC
(10)	Dice	0.85 ± 0.17	0.19 ± 0.09	0.65 ± 0.06	0.67 ± 0.15	0.10 ± 0.06	0.76 ± 0.06
(11)	EUM	0.98	0.61	0.86	1.00	0.80	0.90
(12)	SVM_E^{perf}	0.98	0.51	0.68	1.00	0.80	0.89
(13)	$SVM_{F_1}^{perf}$	0.98	0.59	0.82	1.00	0.80	0.90
(14)	SVM_{ROC}^{perf}	0.61	0.11	0.77	0.67	0.01	0.83

the most noticeable difference being BCE, which is perhaps due to the regularizing effect when using small batches [7].

5 Additional comparisons with other methods of binary classification

5.1 Other baselines

We compare our method with other baselines on the tabular datasets, shown in Table 3. Included in these supplementary results are neural network classifiers trained on Dice [5], Two-Step EUM from [3], and SVM^{perf} [2] to which [6] compares. SVM^{perf} is trained on Errorrate loss (E), F_1 loss (F_1), and AUROC loss (ROC). Our method outperforms the Dice loss in all cases. EUM on the Mammography dataset evaluated on AUROC performs 2 points better than the mean score of our method ($\sigma = 0.03$) and in all other cases our method is the same or outperforms EUM. Our method is comparable or better than SVM^{perf} .

5.2 Two-Step EUM Threshold T and Training-time τ

In this experiment, we applied Two-Step EUM [3], a plug-in method, to our approach and the BCE baseline. Table 4 shows the results of our method, trained with $\tau = 0.5$, compared to the BCE baseline. In the table, T_{max} is the evaluation time threshold that gave the highest score after a search over $T \in \{0.1, \dots, 0.9\}$, evaluated against Accuracy or F_1 -score (columns). During the search for T_{max} , we record the number of threshold that yield the same maximum score, truncated to two significant digits. This count of thresholds is shown in column $|T_{max}|$ in the table. In the case that multiple values of T return the same maximum score, the value of T in the corresponding row shows the value closest 0.5.

Our network performs comparably (within one standard deviation) or better than the BCE baseline. Moreover, in almost every case $|T_{max}|$ for networks trained using our method is equal to or greater than $|T_{max}|$ of the baseline. The exception is the Adult dataset trained on Accuracy using the sigmoid approximation and evaluated on F_1 -score (shown on line (2)) This indicates that our method may be less sensitive to the search for an evaluation-time threshold in the second step of the Two-Step EUM method.

5.3 Weighted loss results

A common method of dealing with sample imbalance is weighting. In this section, we show that our method can also be used with weighting. During training, weighted the loss by the amount of class imbalance in each dataset and compared our method with binary cross entropy. More specifically, we

Table 4: Plug-in Method. See the text for more detail.

Cocktailparty Results ($\mu \pm \sigma$)					
Loss		Accuracy	$ T_{max} $	F_1 -Score	$ T_{max} $
(1)	Accuracy ^l	$0.85 \pm 0.01 @ T = 0.5$	9	$0.72 \pm 0.02 @ T = 0.5$	3
(2)	Accuracy ^s	$0.86 \pm 0.01 @ T = 0.5$	9	$0.72 \pm 0.02 @ T = 0.5$	4
(3)	F_1^l	$0.85 \pm 0.02 @ T = 0.5$	4	$0.77 \pm 0.02 @ T = 0.5$	9
(4)	F_1^s	$0.86 \pm 0.02 @ T = 0.5$	8	$0.77 \pm 0.03 @ T = 0.5$	8
(5)	BCE	$0.87 \pm 0.01 @ T = 0.5$	3	$0.77 \pm 0.02 @ T = 0.5$	2
Adult Results ($\mu \pm \sigma$)					
Loss		Accuracy	$ T_{max} $	F_1 -Score	$ T_{max} $
(1)	Accuracy ^l	$0.81 \pm 0.01 @ T = 0.5$	9	$0.34 \pm 0.06 @ T = 0.5$	5
(2)	Accuracy ^s	$0.81 \pm 0.01 @ T = 0.5$	9	$0.32 \pm 0.11 @ T = 0.5$	1
(3)	F_1^l	$0.75 \pm 0.04 @ T = 0.5$	2	$0.61 \pm 0.02 @ T = 0.5$	9
(4)	F_1^s	$0.76 \pm 0.05 @ T = 0.5$	2	$0.61 \pm 0.03 @ T = 0.5$	9
(5)	BCE	$0.80 \pm 0.01 @ T = 0.5$	2	$0.29 \pm 0.05 @ T = 0.5$	2
Mammography Results ($\mu \pm \sigma$)					
Loss		Accuracy	$ T_{max} $	F_1 -Score	$ T_{max} $
(1)	Accuracy ^l	$0.98 \pm 0.00 @ T = 0.5$	9	$0.00 \pm 0.00 @ T = 0.5$	9
(2)	Accuracy ^s	$0.98 \pm 0.00 @ T = 0.5$	9	$0.00 \pm 0.00 @ T = 0.5$	9
(3)	F_1^l	$0.99 \pm 0.00 @ T = 0.5$	9	$0.68 \pm 0.09 @ T = 0.5$	4
(4)	F_1^s	$0.99 \pm 0.00 @ T = 0.5$	4	$0.70 \pm 0.06 @ T = 0.5$	3
(5)	BCE	$0.99 \pm 0.00 @ T = 0.5$	6	$0.67 \pm 0.08 @ T = 0.5$	1
Kaggle Results ($\mu \pm \sigma$)					
Loss		Accuracy	$ T_{max} $	F_1 -Score	$ T_{max} $
(1)	Accuracy ^l	$1.00 \pm 0.00 @ T = 0.5$	9	$0.00 \pm 0.00 @ T = 0.5$	9
(2)	Accuracy ^s	$1.00 \pm 0.00 @ T = 0.5$	9	$0.00 \pm 0.00 @ T = 0.5$	9
(3)	F_1^l	$1.00 \pm 0.00 @ T = 0.5$	9	$0.81 \pm 0.03 @ T = 0.5$	9
(4)	F_1^s	$1.00 \pm 0.00 @ T = 0.5$	9	$0.82 \pm 0.02 @ T = 0.5$	9
(5)	BCE	$1.00 \pm 0.00 @ T = 0.5$	9	$0.78 \pm 0.07 @ T = 0.5$	3

Table 5: Dataset sample weights. See the text for more details.

Dataset	Negative	Positive
CocktailParty	0.72	1.65
Adult	0.66	2.07
Mammography	0.51	21.55
Kaggle	0.50	290.25

computed sample weights W for each dataset between negative (n) and positive (p) samples where positive samples always correspond to the minority class:

$$W_n = \frac{1}{|n|} \frac{|n| + |p|}{2.0} \quad W_p = \frac{1}{|p|} \frac{|n| + |p|}{2.0}$$

The weights calculated for our datasets are shown in Table 5.

Table 6 shows losses (rows): Accuracy (Acc) and F_1 trained with the sigmoid (s) and linear (l) approximations compared with the traditional binary cross-entropy. Compared to Table 1 in the main paper, results with weighting are very similar. Scores changed the most for the Kaggle dataset. Our method trained on Accuracy with the linear approximation and evaluated on F_1 -Score decreased 8 points. The networks trained on BCE and evaluated on F_1 -Score also decreased, but by 15 points.

Table 6: Weighted loss results. See the text for details.

		CocktailParty ($\mu \pm \sigma$)		Adult ($\mu \pm \sigma$)	
<i>Loss</i>		Accuracy	F_1 -Score	Accuracy	F_1 -Score
(1)	Accuracy ^l	0.84 ± 0.02	0.71 ± 0.03	0.81 ± 0.01	0.35 ± 0.04
(2)	Accuracy ^s	0.84 ± 0.01	0.70 ± 0.03	0.81 ± 0.01	0.34 ± 0.04
(3)	F ₁ ^l	0.86 ± 0.01	0.77 ± 0.02	0.77 ± 0.04	0.61 ± 0.03
(4)	F ₁ ^s	0.86 ± 0.01	0.77 ± 0.02	0.78 ± 0.04	0.61 ± 0.03
(5)	BCE	0.80 ± 0.11	0.72 ± 0.09	0.65 ± 0.21	0.44 ± 0.13
		Mammography ($\mu \pm \sigma$)		Kaggle ($\mu \pm \sigma$)	
<i>Loss</i>		Accuracy	F_1 -Score	Accuracy	F_1 -Score
(1)	Accuracy ^l	0.98 ± 0.00	0.00 ± 0.00	1.00 ± 0.00	0.00 ± 0.00
(2)	Accuracy ^s	0.98 ± 0.00	0.00 ± 0.00	1.00 ± 0.00	0.08 ± 0.23
(3)	F ₁ ^l	0.99 ± 0.00	0.68 ± 0.07	1.00 ± 0.00	0.79 ± 0.03
(4)	F ₁ ^s	0.99 ± 0.00	0.69 ± 0.06	1.00 ± 0.00	0.82 ± 0.03
(5)	BCE	0.91 ± 0.14	0.42 ± 0.21	1.00 ± 0.00	0.50 ± 0.15

Table 7: Data balancing via Oversampling. See the text for more details.

Dataset	Entire Dataset			Oversampled Train Split		
	Total	Positive		Total	Positive	
CocktailParty	4800	1454	30.29%	4284	2142	50%
Adult	48842	11687	23.93%	39564	19782	50%
Mammography	11183	260	2.32%	13970	6985	50%
Kaggle	284807	492	0.17%	363894	181947	50%

Both of these movements are still within one standard deviation. In all cases, our method performs as well or better than the baseline.

Another method of dealing with class imbalance is oversampling. Oversampling is when samples are repeatedly sampled from the minority class until class balance is reached. We applied oversampling to the training split of each dataset. Using this technique we achieved a positive versus negative sample split in each dataset nearer 50/50, detailed in Table 7.

The performance of our method versus the BCE baseline, both with oversampling, is shown in Table 8. In general our method performs better without oversampling. The BCE baseline shows minor improvement compared to weighting. In all cases, our method without oversampling (Table 1 in the paper) performs as well or better than the BCE baseline with oversampling.

5.4 Image data

We also compared the performance of our proposed method to neural network classifiers trained with Dice as the loss function [5]. Results from Dice (logit only) and Dice^s (sigmoid output) are in Table 9. Our method greatly outperformed Dice and DICE^s, likely due to the fact that Dice is designed for image segmentation, rather than binary classification.

6 Balancing between Precision and Recall

Experimental results for balancing between precision and recall as described in Section 5.3 of the main paper are reported in Table 10 for the remaining three tabular datasets. These supplementary results are similar to those presented in the main paper. When directly optimizing F_β -Score while training, $\beta > 1$ typically results in higher Recall than $\beta = 1$. The only exception is the Kaggle dataset, for which we obtained small or no improvement in recall as β increased. We attribute this result to the extreme data imbalance of the Kaggle dataset.

Table 8: Oversampling Results. See the text for more details.

		CocktailParty ($\mu \pm \sigma$)		Adult ($\mu \pm \sigma$)	
	<i>Loss</i>	Accuracy	F_1 -Score	Accuracy	F_1 -Score
(1)	Accuracy ^l	0.84 \pm 0.02	0.74 \pm 0.02	0.71 \pm 0.07	0.60 \pm 0.04
(2)	Accuracy ^s	0.84 \pm 0.02	0.75 \pm 0.02	0.68 \pm 0.09	0.57 \pm 0.05
(3)	F_1^l	0.80 \pm 0.02	0.72 \pm 0.03	0.45 \pm 0.09	0.46 \pm 0.04
(4)	F_1^s	0.80 \pm 0.02	0.73 \pm 0.02	0.51 \pm 0.08	0.49 \pm 0.04
(5)	BCE	0.81 \pm 0.08	0.71 \pm 0.07	0.66 \pm 0.21	0.43 \pm 0.13
		Mammography ($\mu \pm \sigma$)		Kaggle ($\mu \pm \sigma$)	
	<i>Loss</i>	Accuracy	F_1 -Score	Accuracy	F_1 -Score
(1)	Accuracy ^l	0.96 \pm 0.01	0.53 \pm 0.05	1.00 \pm 0.00	0.81 \pm 0.06
(2)	Accuracy ^s	0.97 \pm 0.01	0.55 \pm 0.08	1.00 \pm 0.00	0.81 \pm 0.04
(3)	F_1^l	0.94 \pm 0.02	0.44 \pm 0.07	1.00 \pm 0.00	0.77 \pm 0.05
(4)	F_1^s	0.95 \pm 0.02	0.44 \pm 0.08	1.00 \pm 0.00	0.76 \pm 0.06
(5)	BCE	0.93 \pm 0.07	0.47 \pm 0.17	1.00 \pm 0.00	0.79 \pm 0.06

Table 9: Losses (rows): DICE and DICE^s optimize the DICE coefficient. DICE is logit-only, and DICE^s uses a sigmoid output layer.

CIFAR-10-Transportation Results ($\mu \pm \sigma$)				CIFAR-10-Frog Results ($\mu \pm \sigma$)			
	<i>Loss</i>	Accuracy	F_1 -Score		<i>Loss</i>	Accuracy	F_1 -Score
(6)	DICE	0.521 \pm 0.02	0.625 \pm 0.01	(6)	DICE	0.230 \pm 0.02	0.205 \pm 0.00
(7)	DICE ^s	0.546 \pm 0.04	0.638 \pm 0.02	(7)	DICE ^s	0.277 \pm 0.04	0.216 \pm 0.01

Table 10: Optimizing F_β -Scores ($\beta = \{1, 2, 3\}$) via our method to balance between precision and recall while maximizing F_1 -Score.

CocktailParty F_β -Score Results ($\mu \pm \sigma$)						
<i>Loss</i>	F_1 -Score		Precision		Recall	
	<i>linear</i>	<i>sigmoid</i>	<i>linear</i>	<i>sigmoid</i>	<i>linear</i>	<i>sigmoid</i>
F_1	0.765 \pm 0.02	0.770 \pm 0.02	0.753 \pm 0.03	0.764 \pm 0.03	0.779 \pm 0.04	0.777 \pm 0.03
F_2	0.462 \pm 0.01	0.480 \pm 0.06	0.301 \pm 0.01	0.319 \pm 0.06	1.000 \pm 0.00	0.994 \pm 0.02
F_3	0.465 \pm 0.02	0.473 \pm 0.01	0.303 \pm 0.01	0.310 \pm 0.01	1.000 \pm 0.00	1.000 \pm 0.00
Adult F_β -Score Results ($\mu \pm \sigma$)						
<i>Loss</i>	F_1 -Score		Precision		Recall	
	<i>linear</i>	<i>sigmoid</i>	<i>linear</i>	<i>sigmoid</i>	<i>linear</i>	<i>sigmoid</i>
F_1	0.613 \pm 0.03	0.605 \pm 0.03	0.494 \pm 0.05	0.500 \pm 0.08	0.826 \pm 0.08	0.815 \pm 0.12
F_2	0.425 \pm 0.02	0.426 \pm 0.02	0.270 \pm 0.02	0.271 \pm 0.02	0.997 \pm 0.00	0.996 \pm 0.00
F_3	0.382 \pm 0.00	0.382 \pm 0.00	0.236 \pm 0.00	0.236 \pm 0.00	1.000 \pm 0.00	1.000 \pm 0.00
Kaggle F_β -Score Results ($\mu \pm \sigma$)						
<i>Loss</i>	F_1 -Score		Precision		Recall	
	<i>linear</i>	<i>sigmoid</i>	<i>linear</i>	<i>sigmoid</i>	<i>linear</i>	<i>sigmoid</i>
F_1	0.815 \pm 0.03	0.813 \pm 0.03	0.839 \pm 0.04	0.855 \pm 0.03	0.792 \pm 0.03	0.776 \pm 0.04
F_2	0.824 \pm 0.02	0.805 \pm 0.03	0.849 \pm 0.03	0.819 \pm 0.04	0.803 \pm 0.05	0.793 \pm 0.05
F_3	0.814 \pm 0.03	0.803 \pm 0.02	0.843 \pm 0.05	0.816 \pm 0.03	0.788 \pm 0.03	0.792 \pm 0.03

References

- [1] Dheeru Dua and Casey Graff. UCI machine learning repository, 2017.

- [2] Thorsten Joachims. Training linear svms in linear time. In *Proceedings of the 12th ACM SIGKDD international conference on Knowledge discovery and data mining*, pages 217–226, 2006.
- [3] Oluwasanmi O Koyejo, Nagarajan Natarajan, Pradeep K Ravikumar, and Inderjit S Dhillon. Consistent binary classification with generalized performance metrics. In *NeurIPS*, pages 2744–2752, 2014.
- [4] A. Krizhevsky and G. Hinton. Learning multiple layers of features from tiny images. *Master’s thesis, Department of Computer Science, University of Toronto*, 2009.
- [5] Fausto Milletari, Nassir Navab, and Seyed-Ahmad Ahmadi. V-net: Fully convolutional neural networks for volumetric medical image segmentation. In *2016 fourth international conference on 3D vision (3DV)*, 2016.
- [6] Harikrishna Narasimhan, Rohit Vaish, and Shivani Agarwal. On the statistical consistency of plug-in classifiers for non-decomposable performance measures. In *NeurIPS*, pages 1493–1501, 2014.
- [7] D. Randall Wilson and Tony R. Martinez. The general inefficiency of batch training for gradient descent learning. *Neural Networks*, 16, 2003.
- [8] Kevin S Woods, Jeffrey L Solka, Carey E Priebe, Chris C Doss, Kevin W Bowyer, and Laurence P Clarke. Comparative evaluation of pattern recognition techniques for detection of microcalcifications. In *Biomedical Image Processing and Biomedical Visualization*, 1993.
- [9] Gloria Zen, Bruno Lepri, Elisa Ricci, and Oswald Lanz. Space speaks: towards socially and personality aware visual surveillance. In *Proceedings of the 1st ACM international workshop on Multimodal pervasive video analysis*, pages 37–42, 2010.